Supporting Information
Chang and Jalgaonkar et al.

SI Materials and Methods

Animal studies using Met-1 cells, Lewis Lung Carcinoma (LLC) cells, and a different chemotherapeutic agent cyclophosphamide (CTX). CTX (150 mg/kg in 30 µl PBS) was peritoneally injected on day 4 before tail vein injection of cancer cells (in 200 µl of PBS): Met-1 cells ($2x10^6$) and Lewis Lung Carcinoma (LLC) cells ($5x10^5$). Mice syngeneic to the cancer cells were used: FVB/N mice for Met-1 cells, and C57BL/6 mice for LLC cells. Lung colonies were analyzed on different days post-cancer injection due to their different growth kinetics: 19 or 21 days for Met-1 cells, and 14 days for LLC cells. We used slightly different termination days for the Met-1, due to the difference in the onset of Early Removal Criteria in chemo-treated mice: 19 days for CTX and 21 days for PTX.

Isolation of TEMs and co-culture invasion assay. TEMs ($CD11b^+$ $F4/80^+$ $TIE2^+$) were isolated from the primary tumors in the spontaneous metastasis model on day 26 after cancer cell injection, by fluorescent activated cell sorting (FACS) on a BD FACS Aria II flow cytometer (BD Bioscience) as previously (1) with the same debris exclusion and gating controls as described in the main Method. Within 4-6 hours after isolation, TEMs were co-cultured with cancer cells to test their ability to enhance cancer cell invasion. The BioCoat Tumor Invasion 24-well plate (Corning) that has opaque matrigel embedded insert was used, thus eliminating the need to remove cancer cells on the top of the insert before counting the cells on the underside. tGFP-labeled MVT-1 cells ($5x10^4$) were cultured in the top chamber either alone or with TEMs ($5x10^4$). A chemoattractant gradient was established by using DMEM with 1% FBS in the top chamber and DMEM with 10% FBS in the bottom. Cancer cells on the underside of the matrigel insert were counted at 16 hours after co-culture. For each set of experiment, TEMs from three mice were pooled (to reduce biological variation) and assayed in triplicate wells. Nine images were taken from each well to cover the entire well. To avoid bias, the image files were combined from the three groups (cancer cell alone, cancer cells with WT-Ctl TEMs, and cancer cells with WT-PTX TEMs), coded, and reshuffled (by JDM). This way, the scorer did not have cues for the potential identity of any image due to the cluster it fell in. The images were scored in blind (by SPJ) using pre-determined criteria for what constitutes a true cell signal based on tGFP intensity, size, and shape. The data were decoded (by JDM), and the average cells per field of view (FOV) for each group were calculated.

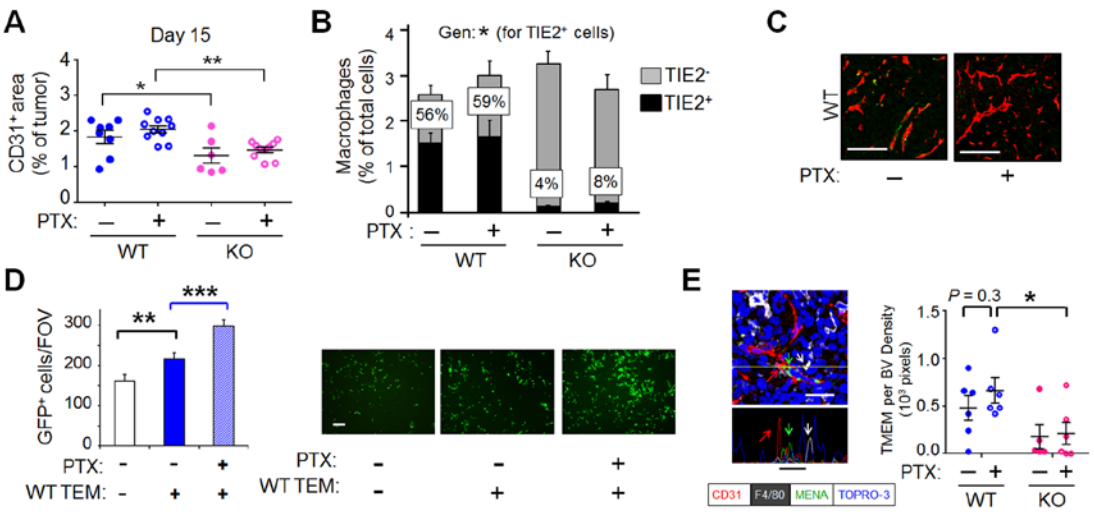

Fig. S1. Analyses of primary tumors. (*A*) The percent (%) of tumor area positive for CD31 in the field of view (FOV) from day-15 tumors was averaged from at least 5 FOVs; each dot represents one tumor (n=8-10, from 3 independent experiments). See Methods for an example of image analysis. (*B*) Day-26 tumors from the spontaneous metastasis model was analyzed by flow cytometry for CD11b, F4/80, and TIE2. Y-axis shows the percent (%) of macrophages ($CD11b^+$, $F4/80^+$) out of total cells in the tumors (no statistically significant difference among the four groups). The $TIE2^+$ cells are represented by the black bars and their mean percent (%) within macrophages is indicated above (n=18, from 6 independent experiments, $P < 0.05$). WT groups were higher than the KO groups but PTX had no effect. (*C*) Representative images of pericyte coverage of day-22 tumors. (*D*) The *in vitro* invasion assay by co-culturing tGFP-labeled MVT-1 cancer cells with TEMs isolated from primary tumors by fluorescent activated cell sorting ($CD11^+$, $F4/80^+$, $TIE2^+$). Left: Numbers of tGFP-labeled cancer cells per field of view (FOV) on the underside of the membrane at 16 hours after culturing without (-) or with (+) of WT TEMs isolated from mice with (+) or without (-) PTX treatment. TEMs from three tumors were combined and assayed in triplicate. The entire underside of the insert were imaged (9 FOVs), and a total 81 of images from three groups of samples (no macrophage, with WT+Ctl or WT+PTX macrophages) were randomized and analyzed in a blind fashion by a different investigator. Data are representative of 2 independent experiments. Right: Representative images. (*E*) TMEM from day-26 tumors was analyzed as that in Fig. 2*E* except antibody against hVEGFA was replaced by antibody against MENA, a protein in the Invasive Signature(2-4) and used previously as a marker for cancer cells to identify TMEM (see main text). Left: A representative image of TMEM is shown; the yellow line denotes the plane for the histogram underneath. The arrows indicate the three cell types that constitute a TMEM: macrophage (F4/80, white), endothelium (CD31, red), and cancer cell (MENA, green). See Methods for details on the identification of TMEM. Blue: TOPRO-3 for nuclear stain. Right: The number of TMEM per blood vessel (BV) density (1,000 pixels) was averaged from 5 or more FOVs for each tumor; each dot represents one tumor (n=6, from 2 independent experiments). More than 120 images were combined from all four groups of mice, randomized, and analyzed in a blind fashion (see Methods). Bars, mean ± SEM; scale bar, 100 μm for (*C* and *D*), 20 μm for (*E*); two-way ANOVA with post-hoc Bonferroni test, except panel (*D*), which is one-way ANOVA with post-hoc Student t test (2-sided); Gen: genotype difference between the corresponding WT and KO; * $P < 0.05$; ** $P < 0.01$; *** $P < 0.001$.

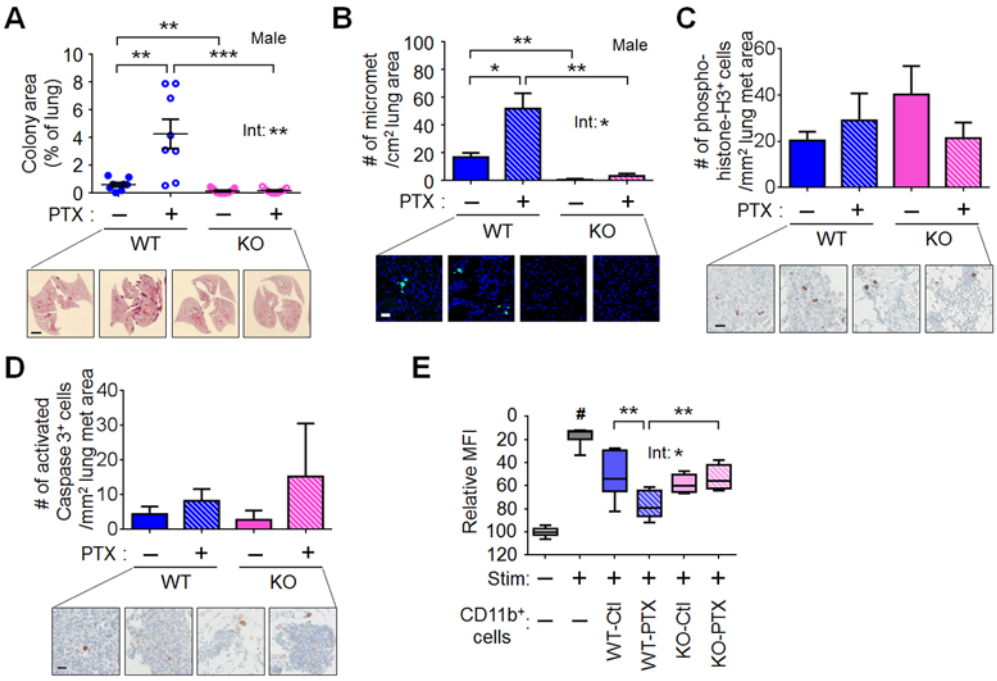

Fig. S2. Analyses of the metastatic lungs. (*A*) Top: Cancer burden in the lung from male mice (day 11 after injection in the lung colonization model) as percent (%) of total lung area (n=8-9, from 3 independent experiments). Bottom: Representative images of H&E stain. Note the lower cancer burden in male mice than female mice (Fig. 4*B*). (*B*) Cancer cell seeding in male mice (day 3 after injection in the lung colonization model). Top: Average numbers of micrometastasis (micromet) per cm^2 lung area. A single or cluster of cells (<5) was counted as one micromet (n=5, from 2 independent experiments). Bottom: Representative images of the tGFP-labeled cells (by immunofluorescent analysis of tGFP). (*C*) Analysis of phospho-histone-$H3^+$ cells in day-26 tumors from the spontaneous metastasis model. Top: Average numbers of positive cells per mm^2 lung metastasis (met) area for each group of mice (n=6). Bottom: Representative immunohistochemical images. (*D*) Same as (*C*) except that activated caspase 3 was assayed (n=6). (*E*) The box-and-whisker plot of the relative median fluorescent intensity (MFI) of the Pacific Blue-A signals from Fig. 5*C* (the T cell suppression assay). Bar, mean ± SEM; scale bar, 2 mm for (*A*), 40 μm for (*B*), 20 μm for (*C* and *D*); Panel (*E*): Box: 25-75 percentile; middle line: median; whiskers: smallest and largest non-outliers; two-way ANOVA with post-hoc Bonferroni test (except for those indicated by #); Int: treatment-genotype interaction; **P*<0.05; ***P*<0.01; ****P*<0.001; # denotes *P*<0.01 between the indicated bar and the other bars in panel (*E*) analyzed by t test (2-sided).

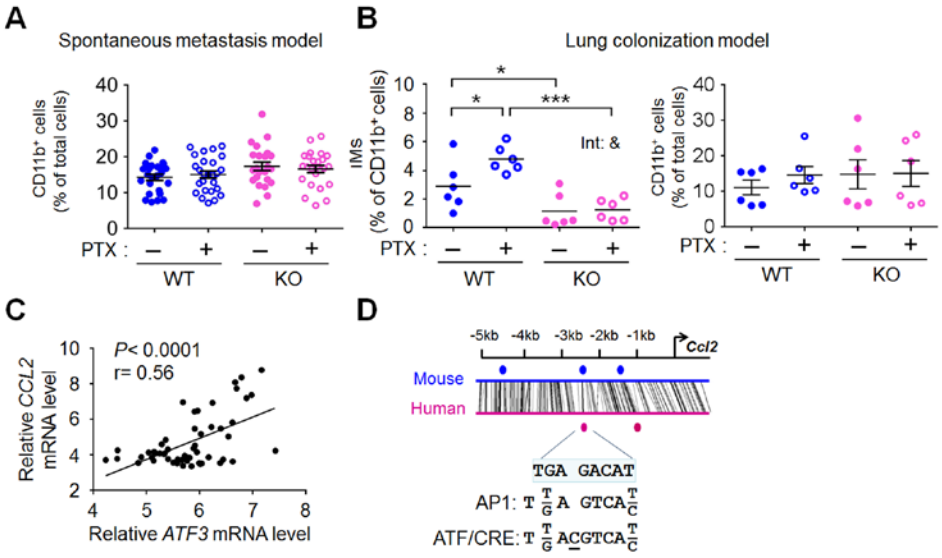

Fig. S3. Analyses of iMs, CD11b+ cells, and CCL2. (*A*) $CD11b^+$ cells expressed as percent (%) in total lung cells derived from the spontaneous metastasis model on day 26 (n=21-26, from 9 independent experiments). (*B*) Left: iMs ($CD11b^+$ $F4/80^+$ $Ly6C^+$ $CCR2^+$) expressed as % in $CD11b^+$ cells using the day-11 lungs from the lung colonization model (n=6, from 2 independent experiments). Right: Same as (*A*) except that samples were from the lung colonization model. (*C*) The correlation between *ATF3* and *CCL2* mRNA levels in 27 human breast cancer cell lines, treated with vehicle (Veh) or PTX (at IC_{50} for each cell line, based on anti-proliferative activity) for 24 hours (data extracted from GEO accession: GSE50811). Y-axis is log base 2 values of spot intensity on the microarray chip after subtracting background signals and normalization. (*D*) A schematics of the mouse *Ccl2* and human *CCL2* promoter with the ATF/CRE, AP-1, and closely related sites indicated. The CONREAL Program was used to analyze the *Ccl2/CCL2* promoter (RefSeq accession NM011333) region from -5,000 to +50 base pairs relative to the transcriptional start site (+1, indicated by an arrow). Up to 2-nucleotide deviation from the ATF/CRE consensus sequence was allowed in order to include ATF/CRE, AP-1, and closely related sites (colored dots), which are potential ATF3-binding sites. The sequence at the -2.3 kb site is indicated and the AP-1 and ATF/CRE consensus sequences are shown for reference. The extra nucleotide in the ATF/CRE site (compared to the AP-1 site) is underlined. two-way ANOVA with post-hoc Bonferroni test; Int: treatment-genotype interaction; **P*<0.05; ****P*<0.001; & *P*=0.08; panel (*C*): Pearson correlation for *P* and r values, the line of best fit by linear regression; kb: kilobases.

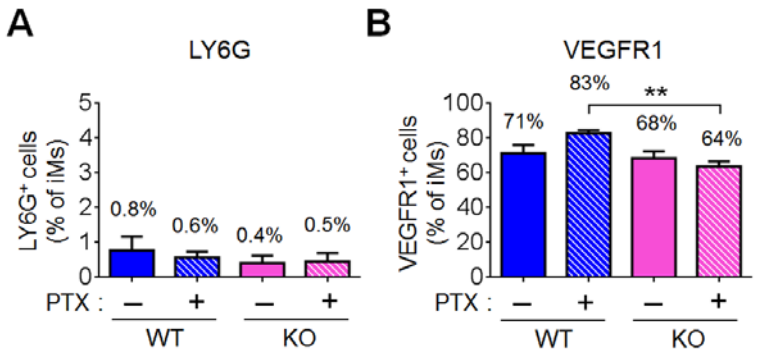

Fig. S4. The majority of iMs from the metastatic lung were negative for LY6G but positive for VEGFR1. (*A*) Metastatic lungs on day 26 from the spontaneous metastasis model were analyzed by flow cytometry for the iM markers ($CD11b^+$, $F4/80^+$, $Ly6C^+$, $CCR2^+$) and LY6G. Y-axis is the percent (%) of $LY6G^+$ cells within iMs, with the average numbers indicated on top of the bars. As shown, most of iMs (>99%) are negative for LY6G (n=8, from 2 independent experiments). (*B*) Same as in (*A*) except VEGFR1was analyzed (n=8, from 2 independent experiments). As shown, most of iMs are $VEGFR1^+$. Bar, mean ± SEM; two-way ANOVA showed no statistically significant difference in the abundance of $LY6G^+$ or $VEGF^+$ cells within iMs, except for WT+PTX versus KO+PTX in $VEGFR1^+$ cells (** $P < 0.01$).

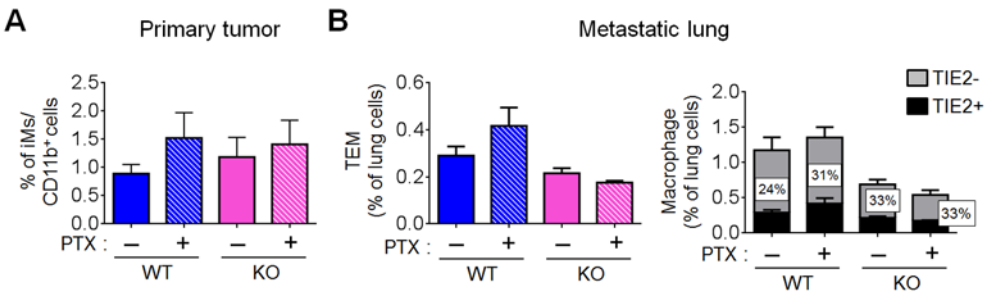

Fig. S5. Comparison of primary tumor and metastatic lung suggested that the *Atf3* genotype and PTX treatment modulated distinct sub-sets of myeloid cells at these two sites. (*A*) iMs ($CD11b^+$, $F4/80^+$, $Ly6C^+$, $CCR2^+$) expressed as percent (%) in $CD11b^+$ cells using day-26 tumors from the spontaneous metastasis model. Two-way ANOVA showed no statistically significant difference among the groups (n=8, from 2 independent experiments). This is in contrast to the metastatic lungs, which showed higher iMs in the WT than ATF3-KO lung, and a further increase by PTX in the WT but not KO lung. (*B*) Metastatic lungs on day 26 from the spontaneous metastasis model were analyzed by flow cytometry for TEM markers (CD11b, F4/80, TIE2). Left: TEMs as percent (%) of total cells in the lungs. Two-way ANOVA showed no statistically significant difference (n=8, from 2 independent experiments). This is in contrast to primary tumors, which showed a genotype difference (more in WT than ATF3-KO counterparts). Right: Y-axis shows the % of macrophages ($CD11b^+$, $F4/80^+$) out of total cells in the lung; black bar represents $TIE2^+$ cells, with the number of $TIE2^+$ cells within macrophages indicated above. In contrast to the primary tumor, $TIE2^+$ cells showed no difference among the groups. Bar, mean ± SEM.

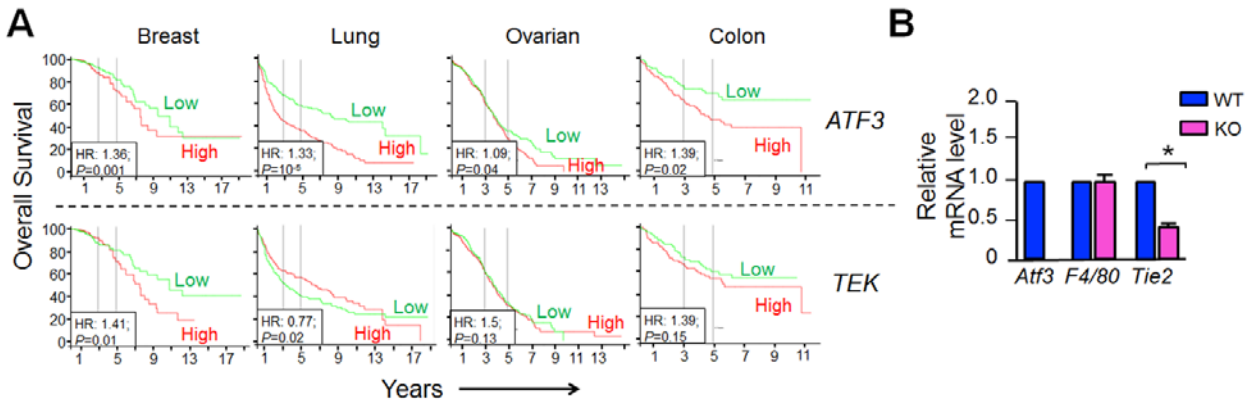

Fig. S6. Expression of *ATF3/Atf3* and *TEK/Tie2* in primary tumors. (*A*) Top: Expression of high *ATF3* correlates with worse outcome in human cancers. Patients with the indicated cancer types from microarray datasets (breast and ovarian cancer: TCGA datasets; lung cancer: GSE30219; colon cancer: GSE17536) were arbitrarily classified into *ATF3*-high (above median) versus *ATF3*-low (below median) group. The online tool PROGgene V2 was used and the Kaplan-Meier curves of their survival are shown. Bottom: Expression of high *TEK* correlates with worse outcome in human cancers. Same as the top panel, except *TEK* (the human ortholog of mouse *Tie2*) was analyzed. Note that the high expression of each gene alone is, in general, a less robust predictor for outcome than the high co-expression of both *ATF3* and *TEK*: lower hazard ratios (HR) and worse *P* values compare to that in Fig. 7*B*. (*B*) Macrophages from WT tumors had higher expression of *Tie2* than that from *Atf3*-KO tumors. Macrophages from day-26 tumors from the spontaneous metastasis model were enriched by MACS beads and analyzed by RT-qPCR for the indicated genes. The signals were standardized against that of actin, and the standardized signals from the WT group was arbitrarily defined as 1 (n=6, from 2 independent experiments). Panel (*A*): Log-rank test; *P* values and HR indicated. Panel (*B*): Bar, mean ± SEM; Student t test (2-sided); **P* < 0.05.

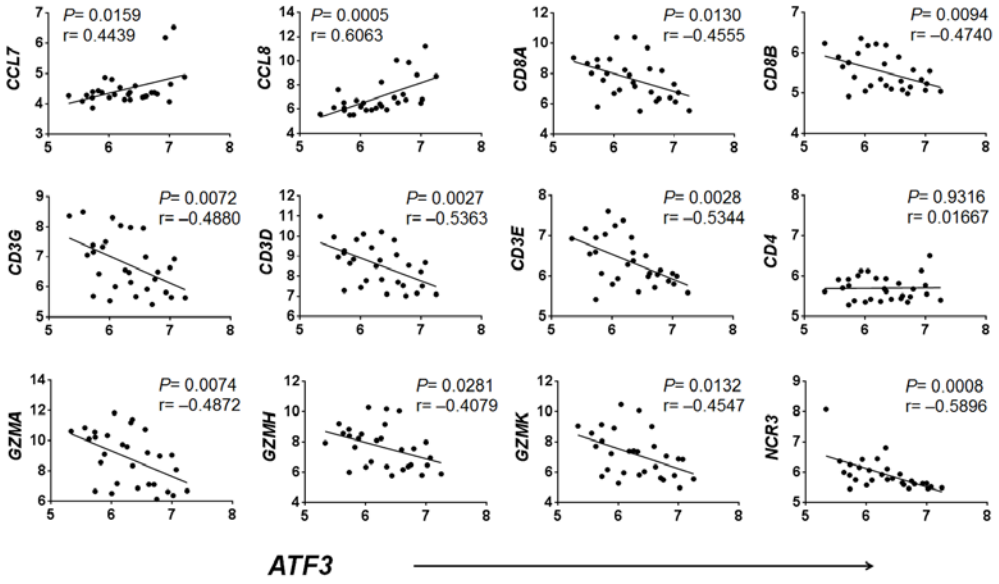

Fig. S7. The correlation of *ATF3* expression with that of the indicated genes in human metastatic samples. Data were extracted from GEO (accession GSE54323), which was derived from breast cancer metastatic sites (including lymph node, bone, and brain, 15 patients, 29 samples). X and Y axes are the relative mRNA level of the indicted genes: log base 2 values of spot intensity on the microarray chip after subtracting background signals and normalization. *ATF3* expression correlated positively with the expression of *CCL7* and *CCL8*, which encode monocyte recruitment factors, but negatively with the expression of markers for cytotoxicity (*GZMA*, *GZMH*, *GZMK*), T cells (*CD3D*, *CD3E*, *CD3G*, *CD8A*, *CD8B*) and natural killer cells (*NCR3*). *ATF3* expression did not correlate with that of *CD4* and the following genes that were analyzed but not shown: *ARG1*, *F4/80*, *LY6G/6C*, *PD-L1*, *CCR2*, *GZMB*, *GZMM*, *XCL1*, *KLRA1*, *NCR1*, *NCR2*, *NCAM1*, and *NCAM2*. Pearson correlation analysis was used and the *P* and r values shown; linear regression for the line of best fit. GZM: Granzyme.

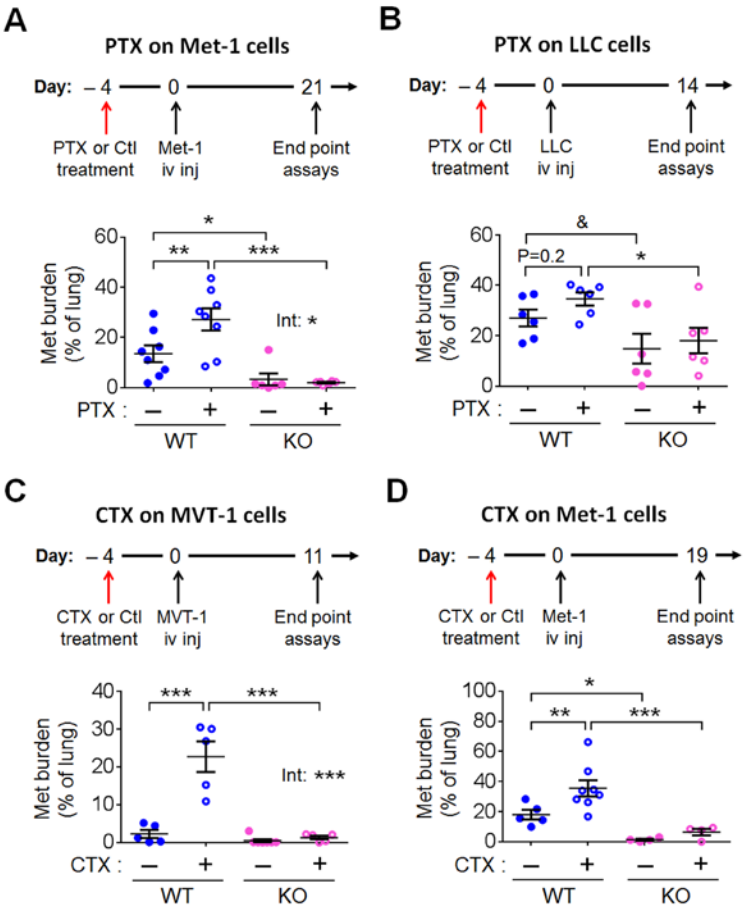

Fig. S8. The effect of PTX on different cancer cells and the examination of a different chemotherapeutic agent cyclophosphamide (CTX). (*A*) PTX (at 25 mg/kg body weight) exacerbated lung colonization of the Met-1 breast cancer cells in the FVB/N mice in a host-*Atf3* dependent manner. Top: A schematic of the experiment. Bottom: The cancer burden in the lung on day 21 as percent (%) of total lung area (n=6-8 from 2 independent experiments). (*B*) PTX exacerbated lung colonization of the Lewis lung carcinoma (LLC) cells in the C57BL/6 mouse in a host-*Atf3* dependent manner. Top: A schematic of the experiment. Bottom: The cancer burden in the lung on day 14 as % of total lung area (n=5-6, from 2 independent experiments). (*C*) CTX, another frontline chemotherapeutic agent, exacerbated MVT-1 breast cancer lung colonization in a host-*Atf3* dependent manner. Top: A schematic of the experiment. Bottom: The cancer burden in the lung on day 11 as % of total lung area (n=5-6). (*D*) Same as panel (*C*) except that Met-1 breast cancer cells were used. Top: A schematic of the experiment. Bottom: The cancer burden in the lung on day 19 as % of total lung area (n=4-8, from 2 independent experiments). Bar, mean ± SEM; two-way ANOVA with post-hoc Bonferroni test; *$P < 0.05$; ** $P < 0.01$; *** $P < 0.001$; & $P = 0.066$.

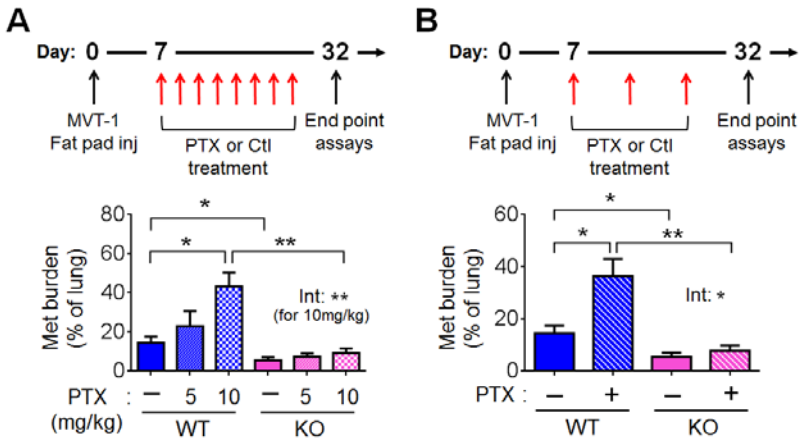

Fig. S9. Different regimens of PTX treatment. (*A*) Control (Ctl) or PTX was used at the same frequency as that in Fig. 1*A* (3 times a week, total 8 injections) but at lower doses than that in the main study (n=5): 5 mg/kg and 10 mg/kg. At 10 mg/kg, PTX exacerbated metastasis in a host-*Atf3* dependent manner. (*B*) PTX was used at 18 mg/kg body weight but at a lower frequency and fewer total number of treatment than that in the main study: once a week for total 3 times (n=13-16). At this regimen, PTX exacerbated lung metastasis in a host-*Atf3* dependent manner. Bar, mean ± SEM; two-way ANOVA with post-hoc Bonferroni test. *$P < 0.05$; ** $P < 0.01$.

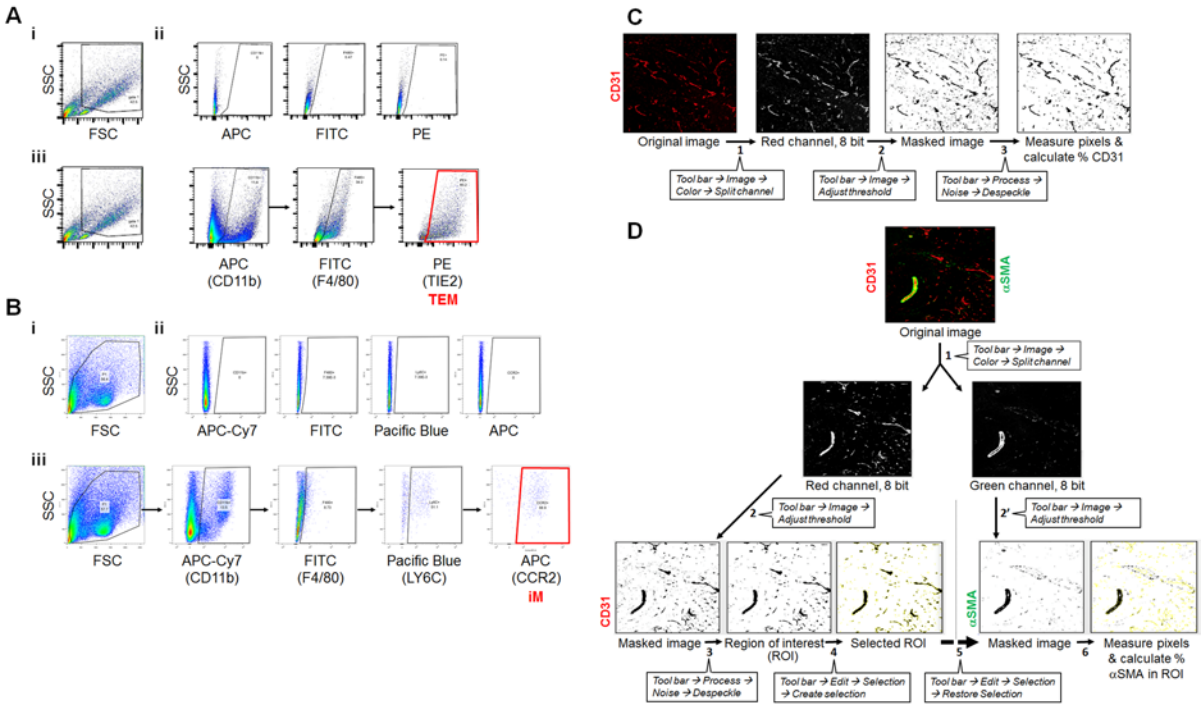

Fig. S10. An example of the gating strategy and imaging analysis. (*A-B*) Gating strategy: (*A*) TEMs from primary tumors. i. FSC and SSC were used in the P1 gate to remove cell debris and large aggregates from the single cell suspension of primary tumor samples. ii. Unstained cells were used to identify cells with background signals. iii. The P1 population of cells was gated sequentially by CD11b, F4/80, and TIE2. (*B*) iMs from the metastatic lungs. i. FSC and SSC were used in the P1 gate as in panel (*A*). ii. Unstained cells were used to identify cells with background signals. iii. The P1 population of cells was gated sequentially by CD11b, F4/80, LY6C, and CCR2. (*C-D*) Imaging analysis: (*C*) Microvascular density. Immunofluorescent image for CD31 stained section (red) was split into red, blue and green channels, and the 8-bit red image was adjusted by the threshold function to create a mask for the area positive for the signal. The pixel number in the mask was divided by the total pixel numbers to obtain the percent of $CD31^+$ cells per FOV. (*D*) Pericyte coverage. Immunofluorescent image for sections stained for CD31 (endothelial cells, red) and ±SMA (pericyte, green) was split into red, blue and green channels. The 8-bit red image was adjusted by the threshold function to create a mask for the area positive for CD31. This mask was used to select the region of interest (ROI), which was applied to the green image to obtain the percent of pericyte coverage ($CD31^+$ cells that are positive for ±SMA) in each FOV.

Chang et al. Table S1. Antibodies used in this study.

Name/Property	Assay/Purpose	Dilution/Amount	Company
anti-ATF3	ChIP	1 µg/500 µL sample	Santa Cruz
anti-CCR2-APC	Flow cytometry	1:20	R&D Systems
anti-CD3µ (clone 145-2C11)	T cell suppression	10 µg/mL	eBioscience
anti-CD4-microbeads	MACS	10 µL/10^7 cells	Miltenyi Biotech
anti-CD8-PE	Flow cytometry	1:100	eBioscience
anti-CD11b-APC-Cy7	Flow cytometry	1:100	eBioscience
anti-CD11b-microBeads	MACS	10 µL/10^7 cells	Miltenyi Biotech
anti-CD16/CD32	Flow cytometry	1:100	eBioscience
anti-CD28 (clone 37.51)	T cell suppression	2 µg/mL	eBioscience
anti-CD45-APC	Flow cytometry	1:100	eBioscience
anti-CD45-micerobeads	MACS	10 µL/10^7 cells	Miltenyi Biotech
anti-cleaved caspase 3 (Asp175) (5A1E)	IHC	1:500	Cell signaling Technology
anti-F4/80-FITC	Flow cytometry	1:100	eBioscience
anti-human VEGF	IF	1:50	Santa Cruz
anti-Ly6C-eFluor450	Flow cytometry	1:100	eBioscience
anti-Ly6G-PE	Flow cytometry	1:100	eBioscience
anti-MENA	IF	1:50	Santa Cruz
anti-Perforin (clone CB5.4)	IHC	1:200	Abcam
anti-phospho-Histone H3 (Ser10)	IHC	1:200	Cell Signaling Technology
Anti-rabbit IgG isotype antibody	ChIP	1 µg/500 µL sample	eBioscience
anti-turboGFP	IF	1:2000	Thermo Scientific

IHC: Immunohistochemistry; IF: Immunofluorescence; ChIP: Chromatin immunoprecipitation

Chang et al. Table S2. Primers used in this study.

Gene	Orientation	Sequence
Adam9	Fwd. Rev.	5’-AAGATTGCCAGTTCCTTCCA-3’ 5’-AACCAAAGATGACCTGACAC-3’
Adam10	Fwd. Rev.	5’-CATTGCTGAGTGGATTGTGG-3’ 5’-TTAAAGTGCCTGGAAGTGGT-3’
Adam15	Fwd. Rev.	5’-CTCCACAGACTTCCTACCAG-3’ 5’-GTCCACAAACATATTTCCACAC-3’
Adam17	Fwd. Rev.	5’-GTGAGAAACGAGTACAGGAC-3’ 5’-GTGATGAAACAGAGACAGGG-3’
Adamts4	Fwd. Rev.	5’-AATTCAGGTATGGATACAGCG-3’ 5’-CAGGTAGATGCTCTTGAGAC-3’
Arg1	Fwd. Rev.	5’-CCAGAAGAATGGAAGAGTCAG-3’ 5’-GGTACATCTGGGAACTTTCCT-3’
Atf3	Fwd. Rev.	5’-GAGATGTCAGTCACCAAGTC-3’ 5’-CAGTTTCTCTGACTCTTTCTGC-3’
Ccl1	Fwd. Rev.	5'-GCCGTGTGGATACAGGATGTT-3' 5'-AAGGTGGCTCATCTTCACCCC-3'
Ccl2	Fwd. Rev.	5'-CAGCAAGATGATCCCAATGAG-3’ 5'-GGTCAACTTCACATTCAAAA-3’
Ccl3	Fwd. Rev.	5'-TGCAACCAAGTCTTCTCAGCG-3' 5'-TTCCTCGCTGCCTCCAAGAC-3'
Ccl4	Fwd. Rev.	5'-CTAACCCCGAGCAACACCAT-3' 5'-GGAGCAAAGACTGCTGGTCTC-3'
Ccl5	Fwd. Rev.	5'-GTGCTCCAATCTTGCAGTCGT-3' 5'-TGAGTGGCATCCCCAAGCTG-3'
Ccl7	Fwd. Rev.	5'-GGAAGCTGTTATCTTCAAGAC-3' 5'-CTAGGTTGGTTTCTGTTCAGG-3'
Ccl8	Fwd. Rev.	5'-GTCAGCCCAGAGAAGCTGACT-3' 5'-AACTTCCAGCTTTGGCTGTCTC-3'
Ccl11	Fwd. Rev.	5'-AGCCATAGTCTTCAAGACCA-3' 5'-GAAAGAGAAGGAATCAAGCAG-3'
Ccl26	Fwd. Rev.	5'-ATGTCCTGCTGCCCTAATTTCAG-3' 5'-CTGGACACAGAATTGCTTACCTG-3'
cMyc	Fwd. Rev.	5’-CTCAGTGGTCTTTCCCTACC-3’ 5’-CTTCTTGCTCTTCTTCAGAGTC-3’
Cxcl10	Fwd. Rev.	5'-CATCCCTGCGAGCCTATCCT-3' 5'-ACGGCTGGTCACCTTTCAGA-3'

Cxcl12	Fwd. Rev.	5'-CCAGAGCCAACGTCAAGCAT-3' 5'-TGAGCCTCTTGTTTAAAGCTTTCTC-3'
Cx_3cl1	Fwd. Rev.	5'-TGGCTTTGCTCATCCGCTAT-3' 5'-CCGCTTCTCAAACTTGCCAC-3'
Csf1	Fwd. Rev.	5'-CCAATGCTAACGCCACCGAG-3' 5'-TGGCTTTAGGGTACAGGCAGT-3'
Il-10	Fwd. Rev.	5'- TTAATAAGCTCCAAGACCAAGG -3’ 5'-TTCCAAGGAGTTGTTTCCGT-3’
Mmp2	Fwd. Rev.	5’-GTTCTGGAGATACAATGAAGTG-3’ 5’-CAGTCTGATTTGATGCTTCC-3’
Mmp3	Fwd. Rev.	5’-TTGAAGCATTTGGGTTTCTC-3’ 5’-CACTTCCTTTCACAAAGACTC-3’
Mmp7	Fwd. Rev.	5'-TGTCACCTACAGAATTGTATCC -3’ 5'-ATGACCTAGAGTGTTCCCTG-3’
Mmp9	Fwd. Rev.	5’-CAGGAGTCTGGATAAGTTGGG-3’ 5’-TCAAGTCGAATCTCCAGACAC-3’
Mmp12	Fwd. Rev.	5’-ACTACTGGAGGTATGATGTG-3’ 5’-CATTCTTCCTAACAACCAAACC-3’
Mmp13	Fwd. Rev.	5’-TTTCTTTATGGTCCAGGCGA-3’ 5’-CACATGGTTGGGAAGTTCTG-3’
Mmp14	Fwd. Rev.	5’-CAAGTGATGGATGGATACCC-3’ 5’-GTGCTTATCTCCTTTGAAGAAGAC-3’
Nos2	Fwd. Rev.	5’-AACCCAAGGTCTACGTTCAG-3’ 5’-GAAATAGTCTTCCACCTGCTC-3’
Tgf beta	Fwd. Rev.	5’-TCACCCGCGTGCTAATGGTGG-3’ 5’-GGTAACGCCAGGAATTGTTGC-3’
TIE2	Fwd. Rev.	5'-CAGGCATTCCAGAACGTGAGA-3' 5'-TCCTGCGAAGTCCCTGTGAT-3'
Timp1	Fwd. Rev.	5’-GATGAGTAATGCGTCCAGGA-3’ 5’-CATCATGGTATCTCTGGTGTG-3’
Timp2	Fwd. Rev.	5’-CTCTGTGACTTCATTGTGCC-3’ 5’-CCCATTGATGCTCTTCTCTG-3’
Tnf alpha	Fwd. Rev.	5’-TGAACTTCGGGGTGATCG-3’ 5’-GCTACAGGCTTGTCACTC-3’
Vegfa	Fwd. Rev.	5'-CCTGGCTTTACTGCTGTACCT-3' 5'-ACTCCAGGGCTTCATCGTTA -3'
Vegfb	Fwd. Rev.	5'-GTGCCTCTGAGCATGGAACT-3' 5'-GTCTGGCTTCACAGCACTCT-3'

Vegfr1	Fwd. Rev.	5'-GAAGACGGTCCTATCGGCTG-3' 5'-TACACGGTGCAAGTGAGGAC-3'
Vegfr2	Fwd. Rev.	5'-GTGGCTAAGGGCATGGAGTT-3' 5'-GCAACACACCGAAAGACCAC-3'
Atf3 for mouse genotyping	Fwd. Rev. #1 Rev. #2	5'-TTCACTGCTAATAGCTCCTG-3' 5'-TTCATAGCTCAGGGAACATCGG-3' 5'-CAACTCCCTCTCCTCAAGTC-3'
Ccl2 (-2.3kb) for ChIP	Fwd. Rev.	5'-TATCTCTCCCGAAGGGTCTGG-3' 5'-TCAGTTAGCACAGGAGGCAG-3'

SI References

1. Wolford CC, *et al.* (2013) Transcription factor ATF3 links host adaptive response to breast cancer metastasis. *J. Clin. Invest.* 123:2893-2906.
2. Wang W, *et al.* (2004) Identification and testing of a gene expression signature of invasive carcinoma cells within primary mammary tumors. *Cancer Res.* 64(23):8585-8594.
3. Wang W, *et al.* (2007) Coordinated regulation of pathways for enhanced cell motility and chemotaxis is conserved in rat and mouse mammary tumors. *Cancer Res.* 67(8):3505-3511.
4. Di Modugno F, *et al.* (2006) The cytoskeleton regulatory protein hMena (ENAH) is overexpressed in human benign breast lesions with high risk of transformation and human epidermal growth factor receptor-2-positive/hormonal receptor-negative tumors. *Clin. Cancer Res.* 12(5):1470-1478.